

# Optimizing Spectral Prediction in MXene-Based Metasurfaces Through Multi-Channel Spectral Refinement and Savitzky-Golay Smoothing

Shujaat Khan<sup>a,b,\*</sup>, Waleed Iqbal Waseer<sup>c</sup>

<sup>a</sup>Department of Computer Engineering, College of Computing and Mathematics, King Fahd University of Petroleum & Minerals, Dhahran, 31261, Saudi Arabia

<sup>b</sup>SDAJA-KFUPM Joint Research Center for Artificial Intelligence, King Fahd University of Petroleum & Minerals, Dhahran, 31261, Saudi Arabia

<sup>c</sup>School of Physics and State Key Laboratory of Electronics Thin Films and Integrated Devices, University of Electronics and Science and Technology of China, Chengdu, 610054, China

## ARTICLE INFO

### Keywords:

Metasurfaces, Multi-Channel Spectral Refinement, Savitzky-Golay Smoothing, Spectral Prediction, Deep Learning

## ABSTRACT

The prediction of electromagnetic spectra for MXene-based solar absorbers is a computationally intensive task, traditionally addressed using full-wave solvers. This study introduces an efficient deep learning framework incorporating transfer learning, multi-channel spectral refinement (MCSR), and Savitzky-Golay smoothing to accelerate and enhance spectral prediction accuracy. The proposed architecture leverages a pretrained MobileNetV2 model, fine-tuned to predict 102-point absorption spectra from  $64 \times 64$  metasurface designs. Additionally, the MCSR module processes the feature map through multi-channel convolutions, enhancing feature extraction, while Savitzky-Golay smoothing mitigates high-frequency noise. Experimental evaluations demonstrate that the proposed model significantly outperforms baseline Convolutional Neural Network (CNN) and deformable CNN models, achieving an average root mean squared error (RMSE) of 0.0245, coefficient of determination  $R^2$  of 0.9578, and peak signal-to-noise ratio (PSNR) of 32.98 dB. The proposed framework presents a scalable and computationally efficient alternative to conventional solvers, positioning it as a viable candidate for rapid spectral prediction in nanophotonic design workflows.

## 1. Introduction

Nanophotonic structures, including photonic crystals, plasmonic nanostructures, and engineered metasurfaces, have demonstrated exceptional capabilities in controlling electromagnetic wave propagation across various spectral ranges [1, 2, 3]. The ability of structurally complex nanophotonic systems to offer optical functionalities that outperform those of natural materials has attracted increasing research interest. Key examples include flat lenses [4] optical vortices [5], plasmon-induced transparency and improved optical imaging [6], Bessel beam generation [7], and perfect absorbers [8]. In addition to these developments, considerable research has focused on engineering a wide variety of absorber geometries for applications in sensing, filtering, and other photonic technologies. However, Metal-insulator-metal (MIM) absorbers, in particular, have gained prominence as efficient platforms for absorption-based applications, such as solar harvesting, thermal emission, and photodetection. These structures exploit the interaction between dielectric and plasmonic resonances, enabling precise spectral tuning through tailored geometric designs [9].

Traditional absorber structures, including plasmonic and semiconductor-based materials, carbon nanotube arrays, and metal–dielectric multilayer films, face challenges by complex integration, high thickness requirements, and complex fabrication procedures. [10, 11, 12]. MXene is two dimensional material represented by the general formula  $M_{n+1}X_nTx$ , consist of transition metal carbides or nitrides with tunable surface terminations, enabling precise control over electromagnetic properties. MXenes based absorbers have garnered considerable attention due to their superior electrical conductivity, broadband absorption characteristics, and ease of integration. Recent studies have demonstrated MXene-based absorbers with enhanced solar absorption and thermal performance compared to conventional materials like carbon nanotubes [11, 12]. Despite their advantages, designing MXene-based absorbers for specific spectral responses remains computationally demanding when using conventional electromagnetic solvers

\*Corresponding author

 shujaat.khan@kfupm.edu.sa (S. Khan)

ORCID(s):

such as Finite-Difference Time Domain (FDTD), Finite Element Method (FEM), or Rigorous Coupled-Wave Analysis (RCWA) [13, 14].

Recent advancements in deep learning have presented promising alternatives for predictive modeling of spectrums [15, 16, 17, 18]. Convolutional neural networks (CNNs), including architectures with deformable convolutional layers, have been proposed to learn mappings between metasurface geometries and their corresponding spectral responses, thereby reducing computational costs and improving prediction accuracy [19, 20, 21]. However, the training of these models from scratch necessitates extensive datasets, which are often costly and time-intensive to generate. Moreover, these approaches may struggle to generalize well to unseen geometric configurations, particularly in scenarios with limited training data.

To address these limitations, transfer learning has emerged as a viable strategy, allowing pretrained networks to be fine-tuned for domain-specific tasks [22]. MobileNetV2 [23], a lightweight CNN architecture originally designed for image classification, has shown significant potential in feature extraction from grayscale images, making it a compelling candidate for spectral prediction in metasurface designs [23]. By leveraging pretrained MobileNetV2 and adapting its architecture for spectral regression, the computational cost and training duration can be significantly reduced while retaining the network's feature extraction capabilities.

In addition to transfer learning, signal smoothing techniques, such as the Savitzky-Golay filter, offer further performance enhancements by mitigating noise in predicted spectra while preserving essential spectral features [24]. The Savitzky-Golay filter applies polynomial fitting over a defined window length, effectively attenuating high-frequency noise and improving prediction stability. Additionally, the proposed model integrates a Multi-Channel Spectral Refinement (MCSR) module that employs multiple 1D convolutional layers to further refine spectral predictions, capturing intricate spectral features that conventional CNNs may overlook.

Thus, this study proposes a hybrid predictive modeling framework that incorporates transfer learning, multi-channel spectral refinement, and Savitzky-Golay smoothing for spectral prediction of MXene-based metasurface absorbers. By integrating these three components, the proposed model aims to (1) reduce the requirement for larger dataset through transfer learning on MobileNetV2 model, (2) enhance spectral prediction accuracy via multi-channel filtering, and (3) improve prediction stability using the Savitzky-Golay filter. Comparative analyses are conducted against baseline models, and comprehensive ablation studies are performed to evaluate the contribution of each module to the overall performance.

## 2. Methodology

The proposed framework integrates a deep learning-based predictive model with Savitzky-Golay smoothing and Multi-Channel Spectral Refinement (MCSR) to enhance the accuracy of spectral predictions for MXene-based metasurfaces. The methodology is structured into several key components, including dataset preparation, model architecture, spectral refinement, training protocol, and evaluation metrics.

### 2.1. Dataset Preparation

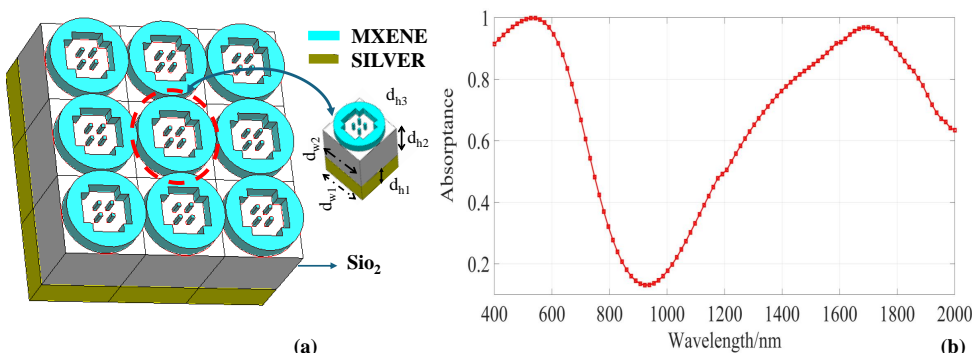


**Figure 1:** (a) Three-layer MIM metasurface-based absorber comprising a top MXene layer, middle  $\text{SiO}_2$  substrate, and bottom silver reflector. (b) Corresponding absorption spectra demonstrating dual-band absorption.

A three-layer metal-insulator-metal (MIM) metasurface absorber was designed, comprising a top MXene layer, a middle  $\text{SiO}_2$  dielectric layer, and a bottom Ag reflective layer, as illustrated in Fig. 1. The MXene layer is 40 nm thick and patterned with 500 distinct geometric designs, each with a spatial resolution of  $100 \times 100$  nm. The intermediate  $\text{SiO}_2$  layer and the Ag reflective layer are both 200 nm thick. The relative permittivity of MXene is based on reported experimental data [10], while  $\text{SiO}_2$  is assigned a constant value of 2.25.

Absorption spectra were computed using CST Microwave Studio under periodic boundary conditions in the x-y plane and open boundaries in the z-direction. A normally incident plane wave was excited to interact with the metasurface. The simulated spectral response was sampled over 102 discrete wavelengths, resulting in a 102-element absorption vector for each design.

The absorptivity  $A(\lambda)$  at wavelength  $\lambda$  was computed as:

$$A(\lambda) = 1 - [R(\lambda) + T(\lambda)], \quad (1)$$

where  $R(\lambda) = |S_{11}|^2$  and  $T(\lambda) = |S_{21}|^2$ . Given the thickness of the Ag reflector, transmission  $T(\lambda) \approx 0$ , thus:

$$A(\lambda) \approx 1 - |S_{11}|^2. \quad (2)$$

The dataset was preprocessed into  $64 \times 64$  grayscale images, representing each metasurface design.

## 2.2. Model Architecture

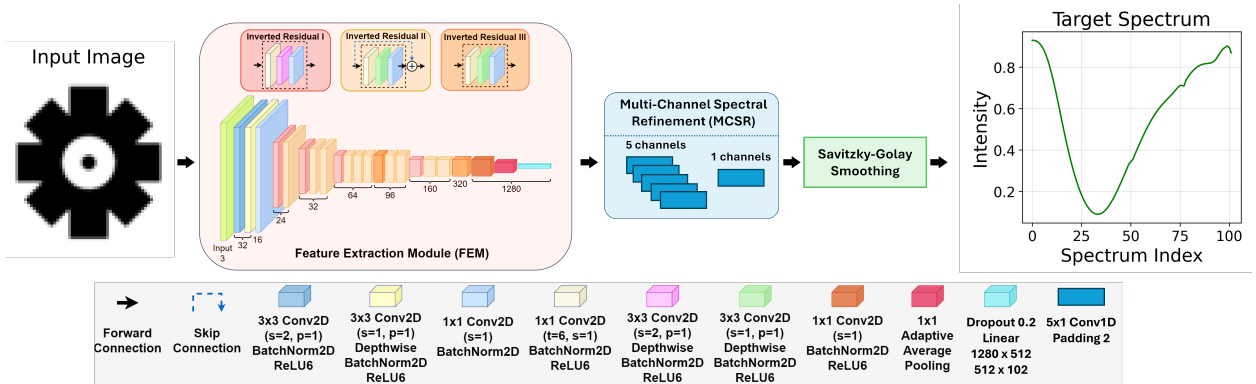


**Figure 2:** Proposed Multi-Channel Spectral Refinement and Savitzky-Golay smoothing framework integrated with MobileNetV2.

The proposed model defined in Figure 2, leverages MobileNetV2 [23], a lightweight deep convolutional neural network originally pretrained on ImageNet. The MobileNetV2 backbone is modified for spectral regression by replacing the fully connected layers with a Multi-Channel Spectral Refinement (MCSR) block, followed by a fixed parameter-based Savitzky-Golay smoothing layer.

For feature extraction, MobileNetV2-based **Feature Extraction Module (FEM)** is designed. The MobileNetV2 backbone was pretrained on ImageNet to extract spatial features. The output feature vector of size 1028 converted to a 512-dimensional representation using a dense layer. Next using another dense layer the 512-dimensional vector is then reduced to a 102-element spectral vector, representing the predicted absorption spectrum.

The 102-element spectral vector was fed to the **Multi-Channel Spectral Refinement (MCSR)** block which consist of two 1D convolutional layers. The first layer expands the single-channel spectral output to five channels and the second layer consolidates the multi-channel output back to a single-channel vector. This structure allows for multi-scale refinement, enhancing spectral fidelity.

To further improve the performance the output of the network was later processed using **Savitzky-Golay Smoothing**. It is applied to the MCSR output to reduce spectral noise. In the proposed approach the filter window length is set to  $W = 11$ , maintaining symmetry about the central data point. While the polynomial order is set to  $d = 2$ , allowing for a quadratic fit to smooth the output spectrum.

### 2.3. Savitzky-Golay Filter Construction

The Savitzky-Golay filter is a digital smoothing filter widely employed in signal processing to reduce noise while preserving the essential features of the signal, such as peaks, troughs, and overall trends. The filter operates by fitting a polynomial to a sliding window of data points using the method of least squares.

#### 2.3.1. Window Length and Symmetry

The filter window length  $W = 11$  is chosen to be an odd integer to maintain symmetry around the central data point. This symmetry ensures effective polynomial fitting, enabling noise reduction while retaining key signal characteristics. The half-window length is defined as:

$$\text{half\_window} = \frac{W - 1}{2} \quad (3)$$

#### 2.3.2. Constructing the Design Matrix

A design matrix  $A$  is constructed using a Vandermonde matrix formulation. The matrix is generated based on the index vector  $x$ , which spans from  $-\text{half\_window}$  to  $\text{half\_window}$ :

$$x = [-\text{half\_window}, -\text{half\_window} + 1, \dots, \text{half\_window}]$$

For a polynomial order  $d = 2$ , the matrix  $A$  is structured as:

$$A = \begin{bmatrix} x_{-n}^d & x_{-n}^{d-1} & \dots & x_{-n} & 1 \\ \vdots & \vdots & \ddots & \vdots & \vdots \\ x_0^d & x_0^{d-1} & \dots & x_0 & 1 \\ \vdots & \vdots & \ddots & \vdots & \vdots \\ x_n^d & x_n^{d-1} & \dots & x_n & 1 \end{bmatrix}$$

where  $n = \text{half\_window}$  and  $d$  is the polynomial degree.

#### 2.3.3. Computation of the Filter Kernel

To determine the Savitzky-Golay filter coefficients, the least squares solution is obtained by computing the pseudo-inverse of the matrix  $A^T A$ :

$$\text{coeffs} = (A^T A)^{-1} A^T \quad (4)$$

The filter kernel is extracted as the first row of the resulting coefficient matrix, effectively representing the weighting coefficients applied to each data point in the window.

Finally the MCSR output signal is convolved with the coefficients to produce smooth output.

### 2.4. Training Protocol

The model is trained using the Adam optimizer [25] with a learning rate of 0.001 and a batch size of 32. The loss function is the Mean Squared Error (MSE), computed as:

$$\text{Loss} = \frac{1}{N} \sum_{i=1}^N (\hat{y}_i - y_i)^2, \quad (5)$$

where  $\hat{y}_i$  and  $y_i$  denote the predicted output from MCSR block and ground truth spectral values, respectively.

Early stopping is implemented to terminate training if validation loss does not improve for 50 consecutive epochs. He initialization [26] is applied to all convolutional layers to stabilize training. Each training run is repeated 10 times, and in each round the dataset was randomly divided into training (80%), validation (10%), and testing (10%) subsets and the mean and standard deviation of the metrics are recorded.

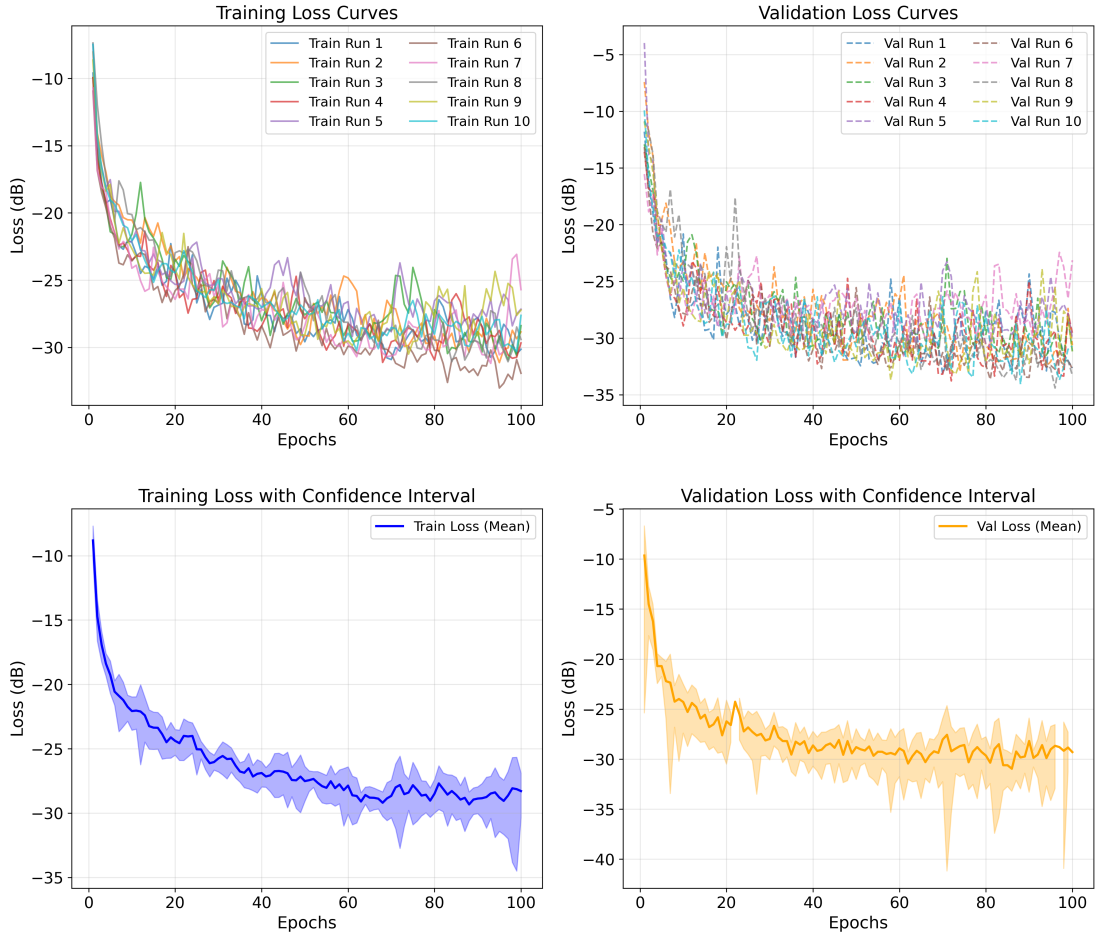


**Figure 3:** (Top): Training (left) and validation (right) loss curves for the proposed model. The (bottom) plots illustrate the confidence interval across multiple runs, indicating consistent performance.

## 2.5. Evaluation Metrics

Model performance was assessed using root mean squared error (RMSE), coefficient of determination ( $R^2$ ) and peak-signal-to-noise-ratio (PSNR). These metrics provide insight into average prediction error and variance explained by the model.

## 2.6. Explainability via Grad-CAM

To interpret the model's predictive focus, Grad-CAM [27] is applied to the final convolutional layer, generating heatmaps that visualize the spatial regions in the input metasurface geometry most influential to the predicted spectral response. These visualizations provide insights into how specific geometrical features affect spectral characteristics.

## 3. Results and Discussion

### 3.1. Training Performance Analysis

The training performance of the proposed framework was evaluated by monitoring the loss convergence across 100 epochs. The learning curves for both training and validation sets are depicted in Fig. 3. The model with transfer learning, multi-channel spectral refinement (MCSR), and Savitzky-Golay smoothing demonstrated a stable convergence pattern with lower mean squared error (MSE) and minimal overfitting, as indicated by the closely aligned training and validation curves.

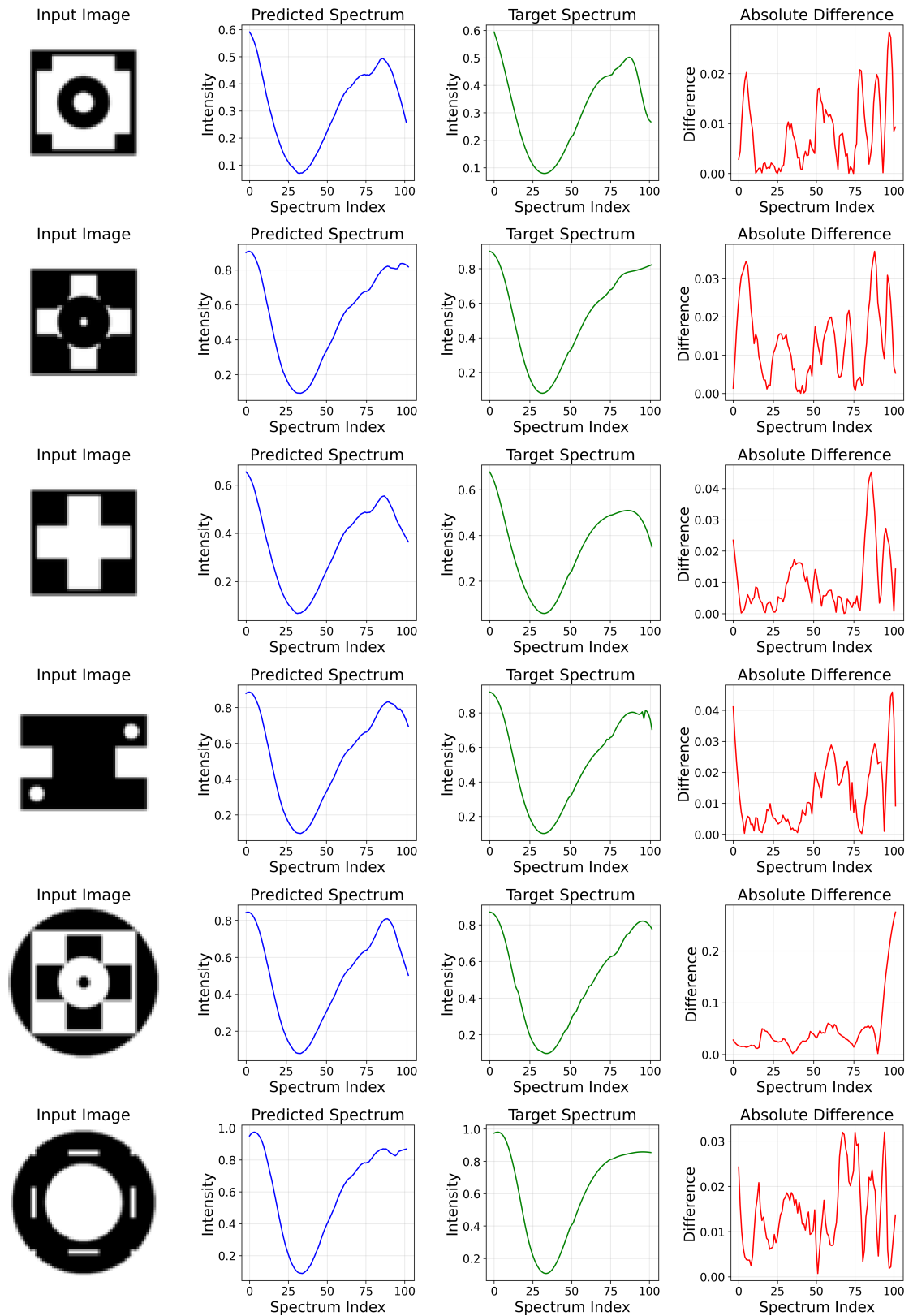


**Figure 4:** Comparison of the predicted vs. actual spectra for six representative metasurface designs. The model accurately captures both broadband and narrowband absorption features, benefiting from the MCSR and smoothing layers.

**Table 1**

Quantitative Performance Metrics for the Proposed Model (with Pretraining + MCSR + Smoothing)

Run #	RMSE ↓	R <sup>2</sup> Score ↑	PSNR (dB) ↑
1	0.0215	0.8949	33.3688
2	0.0209	0.9795	33.5927
3	0.0357	0.9358	28.9416
4	0.0249	0.9739	32.0799
5	0.0285	0.9236	30.9018
6	0.0247	0.9351	32.1313
7	0.0157	0.9860	36.0637
8	0.0201	0.9813	33.9489
9	0.0213	0.9854	33.4393
10	0.0217	0.9823	33.2577
<b>Mean ± Std</b>	<b>0.0245 ± 0.0062</b>	<b>0.9578 ± 0.0305</b>	<b>32.9827 ± 1.8284</b>

**Table 2**

Comparison of Proposed Model with CNN and Deformable CNN

Model	RMSE ↓	R <sup>2</sup> Score ↑	PSNR (dB) ↑
CNN (Baseline) [19]	0.0430 ± 0.0133	0.8883 ± 0.0712	27.86 ± 2.80
Deformable CNN [19]	0.0347 ± 0.0136	0.9010 ± 0.0685	29.57 ± 3.40
<b>Proposed</b>	<b>0.0245 ± 0.0062</b>	<b>0.9578 ± 0.0305</b>	<b>32.98 ± 1.83</b>

### 3.2. Qualitative Evaluation of Spectral Predictions

Qualitative evaluation was performed by comparing the predicted spectra against the ground truth spectra obtained through CST simulations. Six representative metasurface designs were selected, demonstrating varying spectral responses to assess the model's predictive capability (Fig. 4).

The proposed model effectively captured the absorption peaks and troughs across diverse metasurface geometries. The use of transfer learning and multi-channel spectral refinement notably enhanced the spectral resolution, reducing deviations from the ground truth.

### 3.3. Quantitative Evaluation and Model Performance

The quantitative evaluation was conducted by computing the root mean squared error (RMSE), coefficient of determination ( $R^2$ ), and peak signal-to-noise ratio (PSNR) for each run. The detailed performance metrics across 10 runs are summarized in Table 1.

The proposed model exhibited consistent performance across all runs, achieving an average RMSE of 0.0245,  $R^2$  of 0.9578, and PSNR of 32.98 dB. The low standard deviation across runs underscores the model's robustness and generalizability.

### 3.4. Comparison with State-of-the-Art Methods

To assess the efficacy of the proposed approach, a comparative analysis was conducted against conventional CNN and deformable CNN models. Table 2 presents the comprehensive comparison of RMSE,  $R^2$ , and PSNR across three configurations.

The proposed model achieved a 29% reduction in RMSE, 6.3% increase in  $R^2$  and a 3.41 dB increase in PSNR compared to the deformable CNN, highlighting the effectiveness of pretraining and MCSR in refining spectral predictions.

### 3.5. Computational Efficiency Analysis

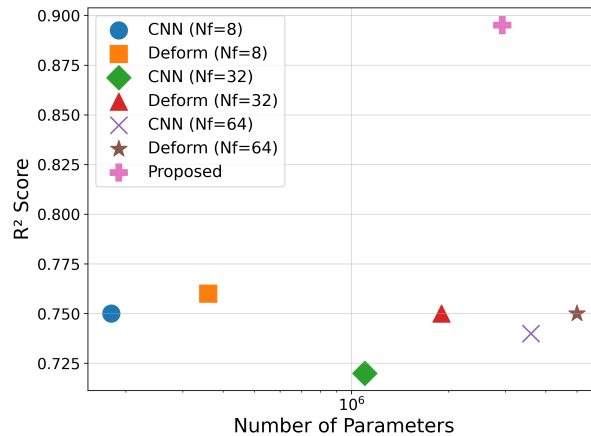


**Figure 5:** Model complexity vs. accuracy: Number of parameters vs.  $R^2$  score for CNN, Deformable CNN, and Proposed Model.

The computational efficiency of the proposed model is evaluated in terms of parameter count and inference speed, and is compared against baseline CNN [19] and Deformable CNN models. The proposed model contains approximately 2.93 million parameters, significantly more than the conventional CNN (1.14 million parameters) but substantially fewer than the Deformable CNN (5.0 million parameters) as reported in [19].

Despite the moderate increase in parameter count compared to the CNN, the proposed model leverages transfer learning and multi-channel spectral refinement to achieve superior spectral prediction accuracy. Specifically, it achieved an  $R^2$  score of 0.9578 with a parameter count of 2.93 million, whereas the Deformable CNN achieved an  $R^2$  score of 0.7492 with 5.0 million parameters [19]. Comparison with other suggested configurations of the baseline CNN and Deformable CNN-based models [19] are depicted in Fig. 6.

### 3.6. Robustness and Explainability via Grad-CAM

The robustness and interpretability of the proposed model were further investigated using Grad-CAM visualizations. Grad-CAM provides a visual representation of the regions within the metasurface geometry that predominantly influence spectral predictions. As depicted in Fig. 6, the model effectively identifies spectral regions that exhibit significant contributions to the absorption spectra, highlighting areas of interest that align with key resonant structures.

The visualizations are structured across four representative metasurface designs, showcasing the model's prediction robustness under varying geometric transformations. The top row in each panel illustrates the original metasurface design, the middle rows present two slightly transformed variants, and the bottom row depicts a substantially altered structure. Despite the geometric variations, the model consistently identifies influential regions, indicating its spatial adaptability and robustness to structural changes.

The Grad-CAM heatmaps reveal that the proposed model not only captures the primary structural features but also emphasizes localized resonant areas that contribute to specific spectral peaks and dips. This ability to visually interpret model predictions enhances its applicability in the design and optimization of MXene-based metasurfaces, enabling researchers to rationalize and refine geometric patterns for targeted spectral responses effectively.

Furthermore, the observed alignment between the Grad-CAM heatmaps and known spectral hotspots confirms that the model leverages physically relevant features for spectral prediction, thereby increasing the overall explainability and reliability of the proposed approach.

### 3.7. Ablation Study and Impact of Smoothing

To assess the contribution of each component — transfer learning, Multi-Channel Spectral Refinement (MCSR), and Savitzky-Golay smoothing — an ablation study was conducted. The results, summarized in Table 3, clearly demonstrate the incremental impact of each module on model performance in terms of RMSE,  $R^2$ , and PSNR.

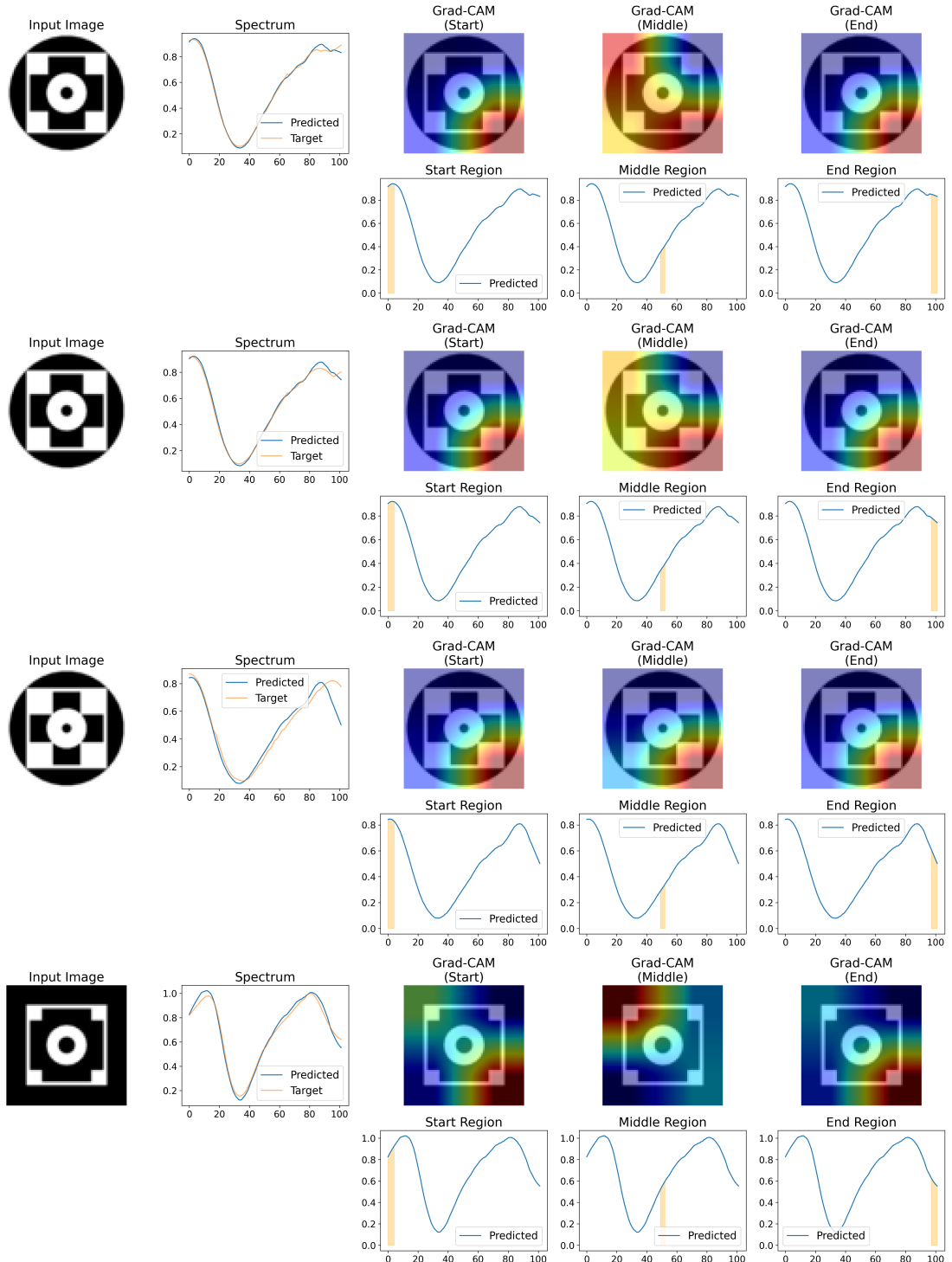


**Figure 6:** Grad-CAM visualizations illustrating the model's focus during spectral prediction across four representative metasurface designs. The top row shows the original design, the middle rows display slightly altered designs, and the bottom row presents substantially transformed structures. Despite geometric variations, the model consistently highlights key spectral regions that influence absorption, demonstrating robustness and interpretability. (Best visible in color print)

**Table 3**

Ablation Study: Effect of Multi-Channel Spectral Refinement, Transfer Learning, and Smoothing on Model Performance

Transfer Learning	MCSR	Smoothing	RMSE ↓	R <sup>2</sup> Score ↑	PSNR (dB) ↑
✗	✗	✓	0.0430 ± 0.0133	0.8883 ± 0.0712	27.86 ± 2.80
✓	✗	✓	0.0310 ± 0.0101	0.9051 ± 0.0548	30.58 ± 2.76
✓	✓	✓	0.0245 ± 0.0062	0.9578 ± 0.0305	32.98 ± 1.83
✓	✓	✗	0.0322 ± 0.0126	0.9031 ± 0.0754	30.29 ± 3.08
✓	✗	✗	0.0347 ± 0.0136	0.9010 ± 0.0685	29.57 ± 3.40

The baseline configuration, consisting solely of smoothing without transfer learning or MCSR, yields the highest RMSE of  $0.0430 \pm 0.0133$ , the lowest  $R^2$  score of  $0.8883 \pm 0.0712$ , and a PSNR of  $27.86 \pm 2.80$ . This configuration serves as a reference point, illustrating the effect of smoothing in isolation.

When transfer learning is introduced without MCSR, the RMSE significantly decreases to  $0.0310 \pm 0.0101$ , and the PSNR improves to  $30.58 \pm 2.76$ . The inclusion of transfer learning enhances the model's feature extraction capabilities by leveraging pretrained weights, leading to substantial gains in spectral prediction accuracy.

The fully integrated configuration — incorporating transfer learning, MCSR, and smoothing — achieves the lowest RMSE of  $0.0245 \pm 0.0062$ , the highest  $R^2$  score of  $0.9578 \pm 0.0305$ , and a PSNR of  $32.98 \pm 1.83$ . These results confirm that the combined effect of all three components maximizes predictive accuracy, reduces noise, and enhances spectral fidelity.

In order to see the effect of smoothing, the smoothing layer is removed from the fully integrated model. With both transfer learning and MCSR applied, the RMSE is dramatically increased to  $0.0322 \pm 0.0126$ , and the PSNR dropped down to  $30.29 \pm 3.08$ . Confirming the importance of the smoothing in fully integrated model.

Lastly, to see the effect of MCSR in isolation, the MCSR block is also removed and only transfer learning was used. With transfer learning alone, the RMSE is further increased to  $0.0347 \pm 0.0136$ , and the PSNR dropped down to  $29.57 \pm 3.40$ . This confirms that the combination of both the MCSR and smoothing enhances spectral refinement, allowing the model to learn and integrate spectral patterns more effectively.

The findings underscore the significant contributions of transfer learning and MCSR in extracting relevant spectral features, while Savitzky-Golay smoothing plays a crucial role in mitigating high-frequency noise and enhancing spectral fidelity. The combined integration of these three components results in optimal model performance, demonstrating the effectiveness of the proposed approach for MXene-based metasurface spectral prediction.

## 4. Conclusion

This study presents a comprehensive deep learning framework for predicting the spectral response of MXene-based metasurface absorbers, integrating transfer learning, multi-channel spectral refinement (MCSR), and Savitzky-Golay smoothing. The proposed model leverages a pretrained MobileNetV2 architecture, effectively adapted to predict 102-point absorption spectra from  $64 \times 64$  grayscale metasurface geometries. Through extensive experimentation, the proposed model demonstrated substantial performance improvements over baseline CNN and deformable CNN architectures, achieving lower RMSE, higher  $R^2$  scores, and superior PSNR values across all evaluated datasets.

The inclusion of MCSR and Savitzky-Golay filtering was pivotal in refining spectral outputs and mitigating noise, thereby enhancing spectral prediction accuracy while maintaining a lightweight model architecture comprising only 2.9 million parameters. Furthermore, the Grad-CAM visualizations provided valuable interpretability, revealing the critical spectral regions influencing the absorption response and aligning well with known resonant hotspots within the metasurface structures.

Future work will focus on expanding the model to handle multi-layered metasurfaces and more complex geometric configurations. Additionally, integrating inverse design methodologies to directly generate metasurface structures for desired spectral responses represents a promising direction for further research. Enhanced interpretability techniques, such as attention mechanisms and layer-wise relevance propagation, will also be explored to provide deeper insights into the model's decision-making process, further consolidating the proposed framework as a comprehensive solution for nanophotonic design and spectral optimization.

## Acknowledgment

Authors acknowledges the support from the King Fahd University of Petroleum & Minerals (KFUPM) under Early Career Research Grant no. EC241027.

## References

- [1] G.-J. Tang, X.-T. He, F.-L. Shi, J.-W. Liu, X.-D. Chen, J.-W. Dong, Topological photonic crystals: physics, designs, and applications, *Laser & Photonics Reviews* 16 (2022) 2100300.
- [2] S. Li, P. Miao, Y. Zhang, J. Wu, B. Zhang, Y. Du, X. Han, J. Sun, P. Xu, Recent advances in plasmonic nanostructures for enhanced photocatalysis and electrocatalysis, *Advanced Materials* 33 (2021) 2000086.
- [3] T. J. Cui, A. Alù, J. B. Pendry, Guest editorial special issue on metamaterials, metadevices, and applications, *IEEE Transactions on Microwave Theory and Techniques* 71 (2023) 3229–3234.
- [4] M. Khorasaninejad, F. Capasso, Metolenses: Versatile multifunctional photonic components, *Science* 358 (2017).
- [5] L. Huang, X. Song, B. Reineke, T. Li, X. Li, J. Liu, S. Zhang, Y. Wang, T. Zentgraf, Volumetric generation of optical vortices with metasurfaces, *ACS Photonics* 4 (2017) 338–346.
- [6] M. A. Naveed, M. A. Ansari, I. Kim, T. Badloe, J. Kim, D. K. Oh, K. Riaz, T. Tauqueer, U. Younis, M. Saleem, et al., Optical spin-symmetry breaking for high-efficiency directional helicity-multiplexed metaholograms, *Microsystems & Nanoengineering* 7 (2021) 5.
- [7] C. Pfeiffer, A. Grbic, Controlling vector bessel beams with metasurfaces, *Physical Review Applied* 2 (2014) 044012.
- [8] N. I. Landy, S. Sajuyigbe, J. J. Mock, D. R. Smith, W. J. Padilla, Perfect metamaterial absorber, *Physical Review Letters* 100 (2008) 207402.
- [9] M. Soni, S. Misra, Machine-learning-assisted design of multiband terahertz metamaterial absorber, *ACS Applied Optical Materials* 1 (2023) 1679–1687.
- [10] Z. Ding, W. Su, F. Hakimi, Y. Luo, W. Li, Y. Zhou, L. Ye, H. Yao, Machine learning in prediction of mxenes-based metasurface absorber for maximizing solar spectral absorption, *Solar Energy Materials and Solar Cells* 262 (2023) 112563.
- [11] K. Mizuno, J. Ishii, H. Kishida, Y. Hayamizu, S. Yasuda, D. N. Futaba, M. Yumura, K. Hata, A black body absorber from vertically aligned single-walled carbon nanotubes, *Proceedings of the National Academy of Sciences* 106 (2009) 6044–6047.
- [12] K. Chen, C. Deng, C. Zou, Z. Zhao, Q. Liu, X. Wang, L. He, F. Gao, W. Zhao, S. Li, Plasmonic hot-hole injection combined with patterned substrate for performance improvement in trapezoidal pin gap microwire self-powered ultraviolet photodetector, *Nano Energy* 104 (2022) 107926.
- [13] W. Yao, J.-M. Jin, P. T. Krein, A highly efficient domain decomposition method applied to 3-d finite-element analysis of electromechanical and electric machine problems, *IEEE Transactions on Energy Conversion* 27 (2012) 1078–1086.
- [14] M. Moharam, D. A. Pommet, E. B. Grann, T. K. Gaylord, Stable implementation of the rigorous coupled-wave analysis for surface-relief gratings: enhanced transmittance matrix approach, *JOSA A* 12 (1995) 1077–1086.
- [15] D. Liu, Y. Tan, E. Khoram, Z. Yu, Training deep neural networks for the inverse design of nanophotonic structures, *Acs Photonics* 5 (2018) 1365–1369.
- [16] S. Park, J. Lee, S. Khan, A. Wahab, M. Kim, Sersnet: Surface-enhanced raman spectroscopy based biomolecule detection using deep neural network, *Biosensors* 11 (2021) 490.
- [17] S. Khan, J. Huh, J. C. Ye, Switchable and tunable deep beamformer using adaptive instance normalization for medical ultrasound, *IEEE Transactions on Medical Imaging* 41 (2021) 266–278.
- [18] S. Park, A. Wahab, M. Kim, S. Khan, Self-supervised learning for inter-laboratory variation minimization in surface-enhanced raman scattering spectroscopy, *Analyst* 148 (2023) 1473–1482.
- [19] W. I. Waseer, M. A. Baqir, M. Saqlain, M. J. Mughal, S. Khan, Predictive modeling of mxene-based solar absorbers using a deep neural network, *Journal of the Optical Society of America B* 42 (2025) 763–772.
- [20] J. Dai, H. Qi, Y. Xiong, Y. Li, G. Zhang, H. Hu, Y. Wei, Deformable convolutional networks, in: *Proceedings of the IEEE international conference on computer vision*, 2017, pp. 764–773.
- [21] X. Zhu, H. Hu, S. Lin, J. Dai, Deformable convnets v2: More deformable, better results, in: *Proceedings of the IEEE/CVF Conference on Computer Vision and Pattern Recognition*, 2019, pp. 9308–9316.
- [22] A. Howard, M. Sandler, G. Chu, Searching for mobilenetv3, *Proceedings of the IEEE/CVF International Conference on Computer Vision* (2019) 1314–1324.
- [23] M. Sandler, A. Howard, M. Zhu, A. Zhmoginov, L.-C. Chen, Mobilenetv2: Inverted residuals and linear bottlenecks, in: *Proceedings of the IEEE conference on computer vision and pattern recognition*, 2018, pp. 4510–4520.
- [24] A. Savitzky, M. J. E. Golay, Smoothing and differentiation of data by simplified least squares procedures, *Analytical Chemistry* 36 (1964) 1627–1639.
- [25] D. P. Kingma, Adam: A method for stochastic optimization, *arXiv preprint arXiv:1412.6980* (2014).
- [26] X. Glorot, Y. Bengio, Understanding the difficulty of training deep feedforward neural networks, in: *Proceedings of the thirteenth international conference on artificial intelligence and statistics*, JMLR Workshop and Conference Proceedings, 2010, pp. 249–256.
- [27] R. R. Selvaraju, M. Cogswell, A. Das, R. Vedantam, D. Parikh, D. Batra, Grad-cam: Visual explanations from deep networks via gradient-based localization, in: *Proceedings of the IEEE International Conference on Computer Vision (ICCV)*, 2017, pp. 618–626.